Stony Brook University

OFFICIAL COPY

The official electronic file of this thesis or dissertation is maintained by the University Libraries on behalf of The Graduate School at Stony Brook University.

© All Rights Reserved by Author.

Density Functional Calculations of Physical Properties of Sodium Oxide

A Thesis Presented

by

Meagan Thompson

to

The Graduate School

in Partial Fulfillment of the

Requirements

for the Degree of

Master of Science

in

Geosciences

(Mineral Physics)

Stony Brook University

December 2011

Stony Brook University

The Graduate School

Meagan Leigh Thompson

We, the thesis committee for the above candidate for the

Master of Science degree, hereby recommend

acceptance of this thesis.

Donald J. Weidner – Thesis Advisor
Distinguished Professor, Geosciences and Director of the Mineral Physics Institute

Robert C. Liebermann, Distinguished Service Professor, Geosciences

Baosheng Li, Research Professor, Mineral Physics Institute

This thesis is accepted by the Graduate School

Lawrence Martin
Dean of the Graduate School

Abstract of the Thesis

Density Functional Calculations of Physical Properties of Sodium Oxide

by

Meagan Leigh Thompson

Master of Science

in

Geosciences

(Mineral Physics)

Stony Brook University

2011

Sodium is the sixth most abundant crustal element; as such, it is found throughout a variety of mineral systems where it is typically represented as an oxide (Na_2O). However, due to high reactivity, neither Na nor Na_2O are naturally occurring and are volatile. The difficulties in acquisition and safe handling present challenges to traditional experiments. However, these difficulties can be overcome by advances in computational methods in solid state physics. While such computational experiments are demanding, the relative simplicity of structure makes Na_2O a reasonable candidate for this type of analysis.

This thesis presents a Density Functional Theory (DFT) based study of Na_2O in both the Local Density Approximation (LDA) and the Generalized Gradient Approximation (GGA). We calculate significant physical properties and find that in cases where experimental data exist, LDA and GGA form lower and upper bounds that bracket experimental values, so while quantities determined using DFT may not be exact, performing calculations within both approximations may at least provide upper and lower bounds. We find that LDA predicts a lattice parameter of 5.398 Å, while GGA predicts 5.583 Å; and cohesive energy is calculated to be 0.7383 and 0.6356 Ry for LDA and GGA, respectively. Electronic band structure calculations yield an LDA band gap of 0.161 Ry and a GGA band gap of 0.143 Ry, both lower than expected for an ionic insulator, but consistent with electronic structure calculations performed by others. Phonon dispersion and phonon density of states (P-DOS) are determined which allows calculation of longitudinal and transverse acoustic wave velocities and elastic constants. Bulk modulus (K) is calculated from both elastic constants and from the second derivative of total

energy vs. volume and found to be consistent with other calculations. Finally, we calculate Debye temperature (Θ_0) to be 559 and 545 K for LDA and GGA, respectively.

In addition to providing previously unrecorded data for Na_2O, our calculations also present an unconventional way of determining the geologically significant but historically computationally expensive elastic constants and bulk modulus from the relatively inexpensive phonon calculations.

TABLE OF CONTENTS

LIST OF FIGURES

LIST OF TABLES

ACKNOWLEDGEMENTS

I would like to thank my adviser, Don Weidner, for his support and patience throughout my academic career. My deepest gratitude goes to Phil Allen and Xiao Shen of the Stony Brook Solid State Physics group for their exhaustive direction and continual questioning that made this particular project a success. Finally, I extend my heartfelt appreciation to John Parise and Lars Ehm of the Mineral Physics Institute who reminded me to know myself at every step of the way.

Chapter 1. Introduction

Sodium plays an important role in Earth Science: it is the sixth most abundant crustal element[1], and it's oxide, Na_2O stands out as the sixth most abundant mantle oxide[2]. As geoscientists, we are familiar with this oxide as a component in mineral systems. In addition, Sodium oxide has technological potential. Like the other alkali metal oxides, it crystallizes in the cubic antifluorite structure, which exhibits fast ion conduction, a property useful in solid-state batteries, gas detectors and fuel cells. However, despite the role it plays in geosciences and its potential technological utility, little experimental work has been focused on Na_2O. Early experiments by Zintl *et al.* determined the room temperature lattice parameter using powder diffraction [3] and cohesive energy was reported in the 67th Handbook of Chemistry and Physics[4], but has been excluded from the online version. Finally, a 1975 Barrie and Street presented Auger and X-ray spectroscopic studies of both sodium metal as well as Sodium oxide [5].

Further examination of Na_2O on its own was virtually non-existent until advances in computational techniques in solid state physics and chemistry made quantum-mechanical/chemical treatment of reasonably sized systems feasible. The first computational experiments on Na_2O were headed by Roetti Dovesi of the Torino group. Using their CRYSTAL code, they calculated binding energy, equilibrium geometry, lattice parameters, elastic constants (C_{ij}), bulk modulus (K), and Γ-point phonon frequencies for Li_2O, Na_2O and K_2O [6]. At that point in time, the CRYSTAL code utilized all-electron potentials and a linear combination of atomic orbitals in the Hartree-Fock approximation (HF-LCAO). Their determined lattice

parameter was overestimated by less than 1% of the experimentally determined lattice parameter [3], which they extrapolated to zero K; calculated cohesive energy was also in excellent agreement with experiment when corrections were added for ionic correlation. However, no experimental data exists for comparison of the central zone phonon frequencies, elastic constants or bulk modulus for Na_2O. Comparison of calculated phonon frequencies of Li_2O with experimental room temperature data shows good agreement, with overestimation of both the IR and Raman active modes by roughly 10-12%; C_{11} was overestimated by 8%, C_{12} by 11%, and C_{44} by less than 1%. This allows us to infer that calculated values for Na_2O may have achieved similar accuracy. No experimental determinations of K are available for comparison for any of the alkali metal oxides. The Shukla group at Max-Planck-Institute tackled Li_2O and Na_2O again at the Hartree-Fock level, this time using Wannier function based orbitals, presenting cohesive energies, lattice constants, and bulk moduli [7]. The calculated lattice parameters and cohesive energies agreed nearly perfectly with Dovesi *et al*. Their calculated K was approximately 3 GPa higher, but still within numerical error of both programs. The Australian team of Mikajlo, Nixon and Ford filled gaps in experimental data with their 2003 Electron Momentum Spectroscopy (EMS) study for Na_2O [8]. EMS was used to determine features of the electronic band structure of the outermost sodium and oxygen bands. The results of the experiment were then compared to *ab initio* LCAO calculations performed using CRYSTAL98, a more recent version of the earlier Torino CRYSTAL code, updated to include Density Functional Theory (DFT) based calculations. Their calculations were performed at both the HF and DFT levels. The DFT calculations were performed using the local density approximation (LDA), the generalized gradient approximation (GGA) and a hybrid GGA functional known as PB03 (which contains a 25% exact HF exchange) for exchange and correlation. They concluded that, while HF does a

reasonably good job of predicting structural features, DFT with the PB03 functional provided the most reliable results when compared to the EMS experiment in all but the band gaps associated with different ions. Most recently, Eithiraj *et al.* calculated the full electronic band structure for the first time, as well as ground state properties for Na_2O using Linear Muffin Tin Orbitals in the tight-binding scheme (TB-LMTO) and the LDA for exchange and correlation [9]. Their ground state properties agreed reasonably well with experiment, exhibiting the predictable errors associated with the local density approximation. However, their electronic band structure interestingly displayed a direct band gap of 2.241 eV which is more characteristic of a semi-conductor than an ionic insulator.

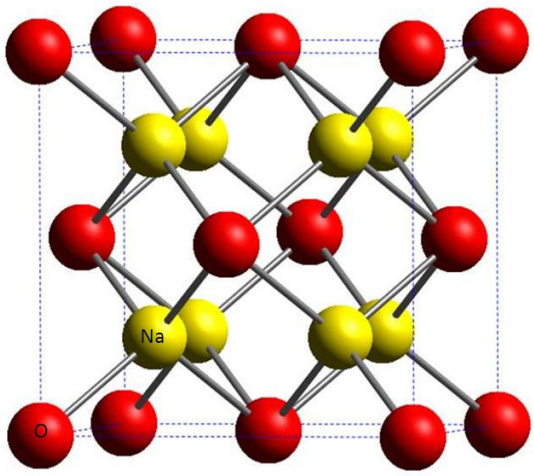

Figure 1.1: FCC crystal structure of Na_2O.
Atomic positions are: O (0, 0, 0); Na (¼, ¼, ¼) and (-¼, -¼, -¼)

While the above computational studies have served to confirm multiple physical characteristics of sodium oxide, they have mainly focused on the alkali metal oxides due to ease of calculation. With a face-centered cubic crystal structure and only 3 atoms and 30 electrons per unit cell, Na_2O lends itself well to computational experiments which become more cumbersome with increased complexity and system size. Most of the calculations performed have been undertaken as a test of the robustness of different algorithms and functionals, not necessarily to test the

nature of the material. The work we have done [10] is, at its core, an attempt to know what is unknown about Na_2O. We approach our calculations from Density Functional Theory with the understanding that it is a robust and well tested approach in materials modeling.

Chapter 2. Methods

2.1 Introduction to First Principles Calculations

While experimental work has set the standard in mineral physics, advances in computing have allowed *ab initio* or "first principles" treatment of mineral systems. The idea of first principles calculations in materials science is to view the many atom system as a many body system composed of interacting electrons and nuclei. From there, the system can be treated from the first principles of quantum mechanics. In this chapter, I will describe the basic concepts of first principle calculations and more detailed information about Density Functional Theory. The information I provide is condensed from multiple sources [11], [12], [13], [14], [15], [16]. There are many computational methods to choose from, each having its own costs and benefits. An overview of all computational methods is outside the scope of this paper, but is treated nicely in Computational Material Science: From *ab initio* to Monte Carlo Methods [13], by Ohno *et al.* In this study, we employ Density Functional Theory (DFT) to determine the ground state properties of Na_2O and Density Functional Perturbation Theory (DFPT) to calculate the phonon spectra.

In classical mechanics, a system of interacting nuclei and electrons can be described by its Hamiltonian, which is a sum of operators that describe the kinetic and potential energy of the system:

$$\hat{H} = T_N + T_e + V_{ee}(\mathbf{r}) + V_{Ne}(\mathbf{r}) + V_{NN}(\mathbf{r})$$

Here T_N and T_e correspond to the kinetic energies of the nuclei and electrons, respectively; while V_{ee}, V_{Ne} and V_{NN} describe the potential energies rising from Coloumbic interactions between

electrons and electrons, nuclei and electrons, and nuclei and other nuclei. In classical mechanics, kinetic energy is described by the momentum (p):

$$\mathrm{T} = \frac{\mathbf{p}^2}{\mathrm{m}}, \text{where } \mathrm{p} = \mathrm{m}\mathbf{v}$$

However, in quantum mechanics, momentum is understood as an operator on the wave function and is written:

$$\mathbf{p} = -\mathrm{i}\hbar\boldsymbol{\nabla}$$

Thus,

$$\mathbf{T}_\mathrm{N} = \frac{\hbar^2\boldsymbol{\nabla}^2}{2\mathrm{M}} \text{ and } \mathbf{T}_\mathrm{e} = \frac{\hbar^2\boldsymbol{\nabla}^2}{2\mathrm{m}}$$

Here, M is the mass of the nucleus and m is the mass of an electron. Now, the Hamiltonian describing our system of interacting nuclei and electrons can be written as a sum of the kinetic and Columbic potential energies:

$$\hat{\mathrm{H}} = -\sum_{\mathrm{I}=1}^{\mathrm{P}} \frac{\hbar^2}{2\mathrm{M}_\mathrm{I}}\boldsymbol{\nabla}_\mathrm{I}^2 - \sum_{\mathrm{i}=1}^{\mathrm{N}} \frac{\hbar^2}{2\mathrm{m}_\mathrm{i}}\boldsymbol{\nabla}_\mathrm{i}^2 + \frac{\mathrm{e}^2}{2}\sum_{\mathrm{i}=1}^{\mathrm{N}}\sum_{\mathrm{j}\neq\mathrm{i}}^{\mathrm{N}} \frac{1}{|\mathbf{r}_\mathrm{i} - \mathbf{r}_\mathrm{j}|} + \mathrm{e}^2\sum_{\mathrm{I}=1}^{\mathrm{P}}\sum_{\mathrm{i}=1}^{\mathrm{N}} \frac{\mathrm{Z}_\mathrm{I}}{|\mathbf{R}_\mathrm{I} - \mathbf{r}_\mathrm{i}|}$$
$$+ \frac{\mathrm{e}^2}{2}\sum_{\mathrm{I}=1}^{\mathrm{P}}\sum_{\mathrm{J}\neq\mathrm{I}}^{\mathrm{P}} \frac{\mathrm{Z}_\mathrm{I}\mathrm{Z}_\mathrm{J}}{|\mathbf{R}_\mathrm{I} - \mathbf{R}_\mathrm{J}|}$$

Where $\mathbf{R} = \{\mathbf{R}_\mathrm{I}\}$, I = 1, 2, …, P, is the set of P nuclear coordinates; and $\mathbf{r} = \{\mathbf{r}_\mathrm{i}\}$, i = 1, 2, …, N, is the set of N electronic coordinates while Z_I is the charge of the I^{th} nucleus. In a crystalline solid, the interest is focused on the calculation of electronic structure. This requires solution of the Schrödinger equation:

$$\hat{H}\boldsymbol{\Psi_i}(\mathbf{R_P}, \mathbf{r_N}) = E\boldsymbol{\Psi_i}(\mathbf{R_P}, \mathbf{r_N})$$

The Hamiltonian is inserted into the Schrödinger equation which is then solved for the ground state wave function: $\boldsymbol{\Psi_i}(\mathbf{R_P}, \mathbf{r_N})$. In practice, this solution is impossible for all but the simplest of systems due to rapidly increasing, coupled degrees of freedom (3N + 3P). In order to get around this, we turn to the Born-Oppenheimer approximation which says that nuclei and electrons exist on such different size and time scales that they can be treated separately thus the full wave function can be factorized into nuclear and electronic portions:

$$\boldsymbol{\Psi}(\mathbf{R}, \mathbf{r}, t) = \boldsymbol{\Theta_m}(\mathbf{R}, t)\boldsymbol{\Phi_m}(\mathbf{R}, \mathbf{r})$$

Where Φ_m (**R, r**) is the electronic wave function and Θ_m(**R,** t) is the nuclear wave function, both at the m^{th} stable state. In our case, this is the ground state, or m = 0. Another effect of the Born-Oppenheimer approximation is that quantum nuclear motion can be neglected allowing nuclei to be treated classically with errors proportional to the anharmonicity of the potential. While this simplifies our problem considerably, it still leaves the formidable issue of how to deal with the electronic many-body problem, which is only analytically solvable for a uniform electron gas and for atoms with few electrons.

2.2 Introduction to Density Functional Theory

Early methods to solve this many-body problem, such as the Hartree (H) and Hartree-Fock (HF) approximations, relied on the *Ansatz* that the many-electron wave function could be written as a product of many one-electron wave functions:

$$\boldsymbol{\Psi}(\mathbf{r_1}, \mathbf{r_2}, \ldots, \mathbf{r_N}) = \boldsymbol{\Phi_1}(\mathbf{r_1}) \ldots \boldsymbol{\Phi_N}(\mathbf{r_N})$$

Each wave function is then a solution to a one-electron Schrödinger equation in an effective potential created by the collection of atomic nuclei and the interactions with the other electrons, by way of a mean-field. A full treatment of the H and HF approximations is outside of the scope of this paper; however, it is worth noting that the HF approximation is also referred to as the *self-consistent-field* (SCF) approximation, which is widely used as the starting point for electronic structure calculations.

The method that could be considered a grandfather of Density Functional Theory (DFT) is the Thomas-Fermi Method (TF). The suggestion in this method was that the quantity of concern in the electronic portion of the Schrödinger equation was not the N-electron wave-function; rather it was the electron density, $n(\mathbf{r})$. Thomas and Fermi were able to formulate a differential equation for the electron density without the introduction of a Hartree-type *ansatz.* This reduced the problem from one depending upon the number electrons in the system and their positions to one of only spatial dependence. The problem that arises from this reduction of variables is one of exchange and correlation. When dealing in electronic density, how do we account for the changes in energy that arise when electrons swap positions? And, how do we account for the movement of all the electrons that occurs when one electron is moved? The TF method made no accounting for this exchange and correlation. The other problems that arose came from the local potential used to describe the kinetic energy, which did a poor job of describing bonding; and from the lack of description for the shell structure of the atom, which led to the incorrect prediction that atoms shrink with increasing atomic number.

The development of DFT began with Hohenberg and Kohn [17], who suggested that the TF method was not incorrect, instead it could be considered an approximation to an exact density functional theory. Their two theorems laid the groundwork for DFT:

1) The ground state energy for a system of electrons acting in an external potential can be uniquely determined by the electron density, n($\mathbf{r}$),

$$E[n] = T_{\mathbf{s}}[n] + \int [V_{\mathbf{ext}}(\mathbf{r}) + U(\mathbf{r})]n(\mathbf{r})\mathbf{dr} + E_{xc}[n]$$

2) The total energy functional E[n] is minimized by the ground state electron density.

In the first theorem, T_s is electron-electron interaction free kinetic energy of a system with density *n,* while U is the Coulomb potential arising from electron-electron interactions. V_{ext} is the external potential from the nuclei and E_{xc} is the exchange and correlation energy. Proof of the Hohenberg-Kohn theorems will not be reproduced in this paper. Instead, we will give an overview of the development of DFT to introduce terms which will be encountered later when we discuss the parameters of our calculations on Na_2O.

Following the general derivation of Mel Levy [18], the Hamiltonian of our interacting N-electron system can now be written:

$$\hat{H} = \hat{T}_{\mathbf{s}} + \hat{U} + \int V_{ext}(\mathbf{r})\hat{n}(\mathbf{r})d\mathbf{r}$$

where $\hat{n}(\mathbf{r})$ is the electron density operator: $\sum_{i=1}^{N} \delta(\mathbf{r} - \mathbf{r}_i)$.

Referring back to the second theorem, the ground state energy is found by minimizing the expectation value of the Hamiltonian over the antisymmetric wave functions

$$E = <\hat{H}> = \min_{\boldsymbol{\Psi}} = \langle \boldsymbol{\Psi} | \hat{H} | \boldsymbol{\Psi} \rangle$$

This minimization can be achieved by redefining the electron density as the expectation value of the electron density: $\langle \hat{n}(\mathbf{r}) \rangle$, which allows the minimization of energy to be broken into two steps:

$$E = \min_{n(\mathbf{r})} \left[F[n] + \int V_{ext}(\mathbf{r}) n(\mathbf{r}) d\mathbf{r} \right]$$

$$F[n] = \min_{\Psi \to n} \langle \Psi | \hat{T}_s + \hat{U} | \Psi \rangle$$

Notice that F[n] formulated in this way is independent of system or external potential, so can be thought of as a universal functional of the electron density.

The electron density we are concerned with is the one that minimizes the total electronic energy. Thus, the optimal electron density is found by applying the Euler-Lagrange equation to the density functional F[n], which gives:

$$\frac{\delta F}{\delta n(\mathbf{r})} + V_{ext}(\mathbf{r}) = \mu$$

Where, μ is the Legrange multiplier corresponding to the constant particle number of the system and $\frac{\delta F}{\delta n(\mathbf{r})}$ is a functional derivative.

From here, an effective potential is established:

$$V_{eff}(\mathbf{r}) = V_{ext}(\mathbf{r}) + \int 2 \frac{n(\mathbf{r}')}{|\mathbf{r} - \mathbf{r}'|} d\mathbf{r} d\mathbf{r}' + V_{xc}(n)$$

This effective potential takes into consideration the external potential from the nuclei, the Hartree potential and the potential arising from the exchange and correlation we spoke of in the

discussion of the TF method. For noninteracting particles, the Schrödinger equation is known as the Kohn-Sham equations.

$$[-\boldsymbol{\nabla}^{\mathbf{2}} + \mathrm{V_{eff}}(\mathbf{r})]\boldsymbol{\Psi}_{\mathbf{i}}(\mathbf{r}) = \epsilon_{\mathrm{i}}\boldsymbol{\Psi}_{\mathbf{i}}(\mathbf{r})$$

ϵ_i are referred to as one-electron Kohn-Sham energies and the corresponding density functional F[n] is:

$$\mathrm{F[n]} = \mathrm{T_s[n]} + \int\int \frac{\mathrm{n}(\mathbf{r})\mathrm{n}(\mathbf{r}')}{|\mathbf{r}-\mathbf{r}'|}\mathrm{d}\mathbf{r}\mathrm{d}\mathbf{r}' + \mathrm{E_{xc}[n]}$$

where E_{xc} is the exchange and correlation energy arising from a system of interacting electrons with a density n(r). Upon solution of the Kohn-Sham equations, the total electronic charge density is calculated as

$$\mathrm{n}(\mathbf{r}) = \sum_{\mathbf{i=1}}^{\mathbf{N}} \boldsymbol{\Psi}_{\mathbf{i}}^{*}(\mathbf{r})\boldsymbol{\Psi}_{\mathbf{i}}(\mathbf{r})$$

Finally, the total energy is calculated:

$$\mathrm{E[n]} = \sum_{\mathrm{i=1}}^{\mathrm{N}} \epsilon_{\mathrm{i}} - \int\int \frac{\mathrm{n}(\mathbf{r})\mathrm{n}(\mathbf{r}')}{|\mathbf{r}-\mathbf{r}'|}\mathrm{d}\mathbf{r}\mathrm{d}\mathbf{r}' - \int \mathrm{V_{xc}}(\mathbf{r})\mathrm{n}(\mathbf{r})\mathrm{d}\mathbf{r} + \mathbf{E_{xc}[n]}$$

Within DFT, a relationship has been established between an interacting system of electrons and a simplified non-interacting system. The relationship is exact in that the density of the non-interacting system is equal to the density of the interacting system. All of the terms which cannot be treated exactly have been displaced onto exchange and correlation effects, the forms of which are unknown.

2.3 Exchange and Correlation

Despite the fact that the exact forms of E_{xc} and V_{xc} are unknown, we can construct an exchange-correlation energy based on things we do know. First, that electron movement obeys the Pauli exclusion principle; secondly, that electrons are repulsed by one another. This creates a so-called exchange-correlation hole which is an area around an electron that cannot be occupied by any other electron. In this construction, exchange-correlation energy arises from the interaction between an electron and its hole.

$$E_{xc}[n(\mathbf{r})] = \int n(\mathbf{r})\epsilon_{xc}[n(\mathbf{r})]d\mathbf{r} = \int n(\mathbf{r})d\mathbf{r} \int \frac{n_{xc}(\mathbf{r},\mathbf{r}')}{|\mathbf{r}-\mathbf{r}'|} d\mathbf{r}'$$

Here, ϵ_{xc} refers to the exchange-correlation energy density which is expressed in terms of the exchange-correlation hole density, $n_{xc}(\mathbf{r},\mathbf{r'})$. Assuming that the exchange-correlation hole density can be split into separate effects, $n_{xc}(\mathbf{r},\mathbf{r'}) = n_x(\mathbf{r},\mathbf{r'}) + n_c(\mathbf{r},\mathbf{r'})$, the following sum rules must hold true:

1. An electron is surrounded by an effective positive volume created by the absence of negative charge

$$n_{\mathbf{x}}(\mathbf{r},\mathbf{r}') \leq 0.$$

2. Each exchange hole can contain only one electron at all r

$$\int n_x(\mathbf{r},\mathbf{r}')d\mathbf{r}' = -1$$

3. Correlation only moves electrons so the number of particles stays constant

$$\int n_c(\mathbf{r},\mathbf{r}')d\mathbf{r}' = \mathbf{0}$$

Jones and Gunnarsson showed that, by making the substitution **R = r – r'**, E_{xc} is dependent on the spherical average of n_{xc}(**r, R**) [19]. This means that the exchange-correlation energy provides a reasonable estimation even for the nonspherical parts of n_{xc}.

From here, there are several different ways to describe the character of the exchange-correlation interactions. In our research, we use two approximations which are known to systematically over and underestimate ground state properties to obtain results which provide upper and lower bounds.

2.3.1 The Local Density Approximation

The Local Density Approximation (LDA) is built on the assumption that the exchange and correlation energy of an electron located at **r** is equal to that of a homogeneous electron gas with an average density equal to the local electron density n(r), or $\epsilon_{xc}^{LDA}[n(\mathbf{r})] = \epsilon_{xc}^{hom}[n(\mathbf{r})]$. This approximation, though simple, offers an exact description for cases where electron density is uniform or varies slowly. It has also worked well for accurately predicting some properties of crystals, like bond lengths, bond angles, vibrational frequencies as well as elastic and bulk moduli; but does tend to overbind, underestimate lattice parameters by 1% - 5% as well as underestimate the band gaps in insulators and semi-conductors [12]. Many of the problems that arise from the LDA come from the simplified view of electron density as uniform.

2.3.2 The Generalized Gradient Approximation

The Generalized Gradient Approximation (GGA) can be thought of as an expansion on the LDA. Where the LDA assumes a uniform electron density, the GGA incorporates a gradient of the electron density and E_{xc} is written in the following form:

$$E_{xc}[n(\mathbf{r})] = \int n(\mathbf{r})\epsilon_{xc}[n(\mathbf{r})]d\mathbf{r} + \int F_{xc}[n(\mathbf{r}), \nabla n(\mathbf{r})]d\mathbf{r}$$

where, F_{xc} must satisfy conditions for the exchange-correlation hole. There is no unique method to satisfy the conditions, so a variety of recipes have been proposed. For the purposes of our research, we use the Perdew-Burke-Erzerhof (PBE) exchange-correlation functional [20]. This particular functional is ideal because it retains the correct features of the LDA while including the most energetically important features arising from the inhomogeneity of the electron density [11]. GGA improves binding and atomic energy as well as bong lengths and angles. It tends to underestimate lattice parameter and does not make appreciable improvements to the band gap problem.

2.4 Parameters of Calculations for Na_2O

The work presented determines lattice parameter, cohesive energy, electronic band structure, phonon spectra, phonon density of state (pDOS), elastic constants, bulk modulus, Debye temperature, and specific heat using the plane wave self-consistent field (PWscf) code. PWscf is part of the QUANTUM ESPRESSO [21] distribution which is a set of open source codes which solves the self-consistent Kohn-Sham equations for a periodic solid within a DFT framework. A plane-wave basis set is used to expand the atomic orbitals and we use Vanderbuilt ultrasoft pseudo potentials [22] with both the LDA and GGA to account for exchange and correlation. For LDA, the Perdew-Zunger (PZ) [23] exchange-correlation energy formulation is used, while we use the Perdew-Burke-Erzerhof (PBE) [20] for the GGA. The sodium pseudopotential includes the $2s^2 2p^6 3s^1$ basis orbitals and the oxygen the $2s^2 2p^4$.

Convergence tests were performed to determine the optimal energy cutoffs and size of k-point grid. For both the LDA and GGA calculations, the energy cutoffs are 30 Ry for wave functions and 420 Ry for charge density. 10x10x10 Monkhorst-Pack k-point grids are used. Figures 2.1 and 2.2 show the convergence tests for LDA and GGA, respectively. The error associated with both energy cutoffs and k-point sampling is 0.002 Ry.

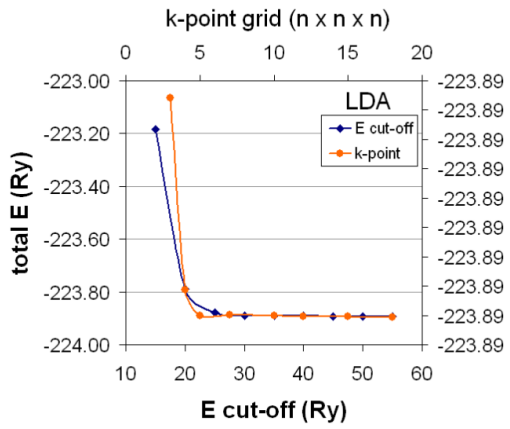

Figure 2.1: Convergence tests for LDA.

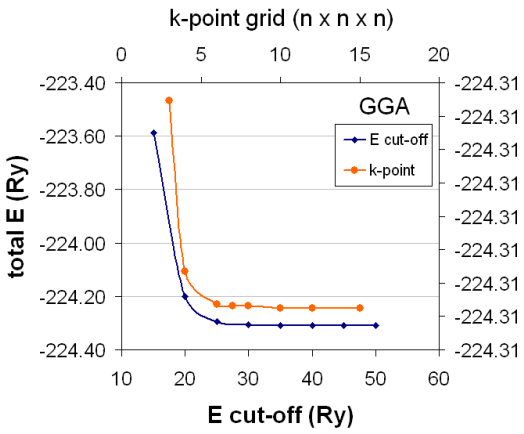

Figure 2.2: Convergence tests for GGA

Chapter 3. Results

3.1 Lattice Parameter and Cohesive Energy

We began by calculating lattice parameter (a). Structures were relaxed to equilibrium at different lattice parameters and then total energy was plotted as a function of lattice parameter. Figure 3.1 shows third order polynomial fits for both LDA and GGA. Lattice parameter was chosen by minimizing the first derivative of the associated polynomial.

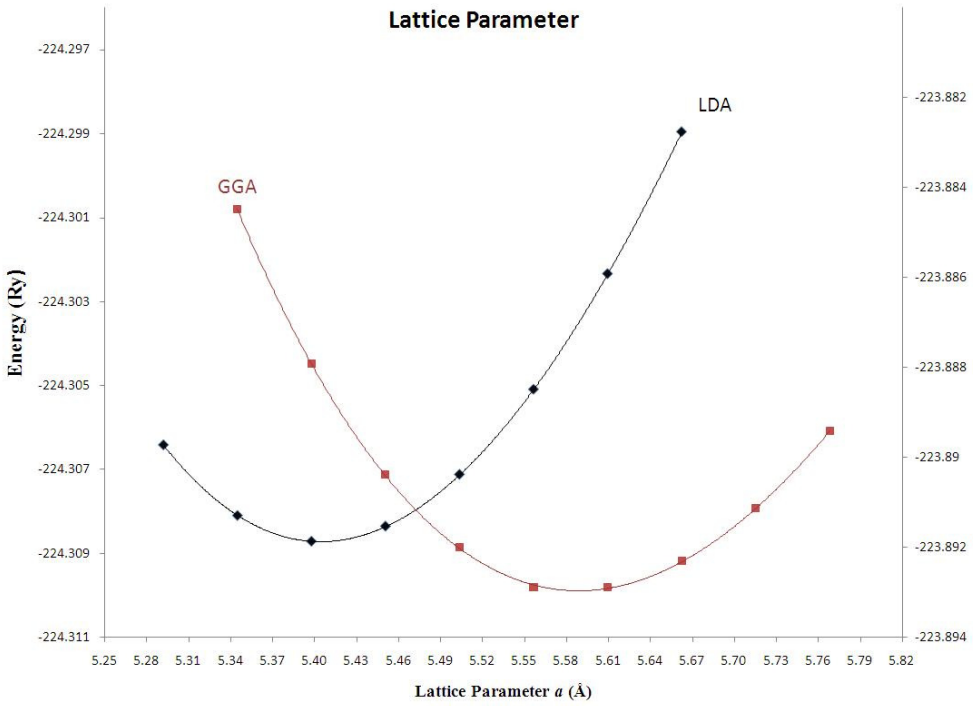

Figure 3.1: Energy plotted as a function of lattice parameter (a). Energies associated with LDA appear on the left y-axis while those associated with GGA are on the right y-axis.

A comparison of our results for lattice parameter and cohesive energy with others is reported in table 3.1. As expected, LDA underestimates lattice parameter (5.398 Å), while GGA overestimates (5.556 Å), resulting in lattice parameters that bracket the experimental 0 K extrapolated lattice parameter of 5.49 Å by approximately 1% in either direction. These results are consistent with what we would expect and are in good agreement with similar studies so provide a foundation for the rest of our calculations.

	Method	*a* (Å)	E_{coh} (Ry)
Expt.		5.49[6]	0.6442[4]
This Study	LDA	5.398	0.7383
	GGA	5.583	0.6356
Mikajlo[8]	LDA	5.393	
	GGA	5.559	
	PBE0	5.498	
Eithiraj[9]	TB-LMTO	5.465	
Dovesi[6]	LCAO	5.484	0.6642
Shukla[7]	HF	5.481	0.3766

Table 3.1: Comparison of lattice parameters and cohesive energies from experiment and calculations.

Energy considerations are important in the calculation of physical properties and cohesive energy is a good test of the quality of your functional in *ab initio* calculations. Cohesive energy is defined as the energy that has to be added to a crystal to separate it into neutral free atoms at rest and is calculated:

$$E_{coh} = E_{tot} - \sum_{A} E_{A}$$

Where E_{tot} is the equilibrium total energy of a crystal and E_A is the sum of the total energies of the free atoms at equilibrium. For this study, we used the total energy of the optimized lattice from table 4.1; atomic energies were calculated in a 10 Å supercell with spin-polarized atoms, assuming atomic oxygen. Referring back to Table 4.1, notice the overbinding

apparent in LDA, which overestimates cohesive energy by about 15%. This overbinding is corrected to a large extent by the GGA functional which underbinds, but only by about 1%. These results are consistent with our expectations and give us confidence in the quality of our functionals.

3.2 Electronic Band Structure

The electronic band structure of a solid plays an important role in understanding the properties of the material. The band structure not only provides a useful way for determining the electrical conductivity of a material, it can also allow for prediction of optical properties.

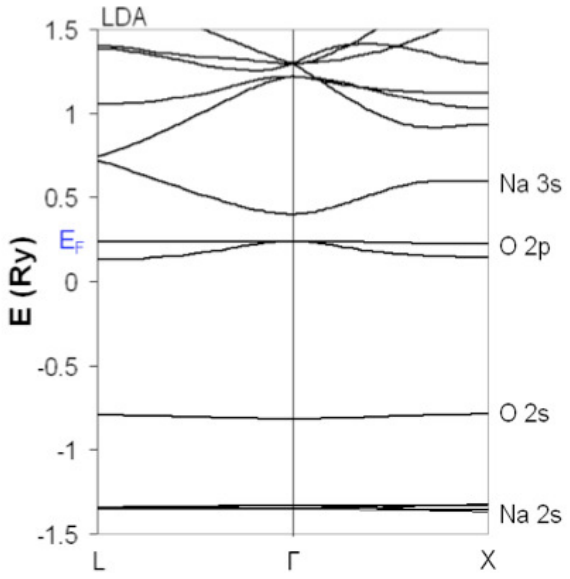

Figure 3.2: Electronic band spectra around the Γ-point

The occupied bands show very little dispersion; calculated data are in reasonable agreement with experimental data and in good agreement with other calculations. The band structure plots between LDA and GGA are almost identical, thus Figure 3.2 shows our calculated electronic band structure within the LDA around the center of the Brillouin zone. Figure 3.2.1 provides an illustration of the f.c.c. Brillouin zone for reference. The band gap is direct at the Γ point and is between the cation "p"-like valence band and the anion "s"-like conduction band. At

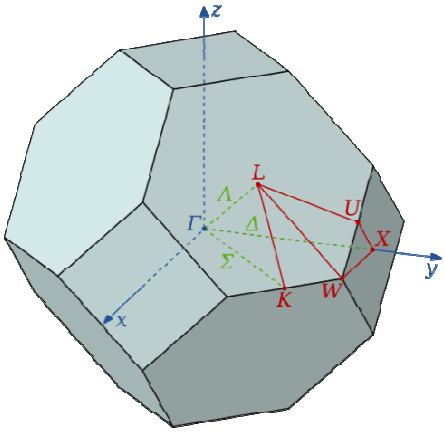

Figure 3.2.1: f.c.c Brillouin zone [24]

0.161 Ry (2.19 eV), the band gap is smaller than expected for an ionic insulator but is consistent with the gap calculated by Eithiraj *et al.* and with what we would expect from the LDA. However, no experimental data exist for comparison. Table 3.2 presents selected key energies from the electronic band structure calculations.

		This Study		**Mikajlo [8]**			**Eithiraj [9]**
	Expt [8]	LDA	GGA	LDA	GGA	PBE0	TB-LMTO
O 2*p* – O 2*s*	1.165	1.055	1.073	1.046	1.078	1.777	
O 2*s* – Na 2*p*	0.863	0.515	0.530	0.542	0.537	0.568	
Na 2*p* – Na 2*s*	2.315	2.007	2.051	2.015	2.059	2.188	
E_g		0.161	0.143				0.178
W (O 2*p*)	0.044	0.044	0.045	0.074	0.071	0.079	0.036
W (O 2*s*)		0.027	0.019	0.024	0.023	0.025	

Table 3.2 Comparison of selected key energies (Ry) from experiment and other calculations

3.3 Phonon Spectra, Phonon Density of States (pDOS) and related calculations

Phonon spectra and pDOS can give us a wealth of information about the thermoelastic properties of a material. Figure 3.3 presents the first determination of phonon spectra and pDOS for Na_2O along selected paths in the Brillouin zone (refer to Fig 3.2.1). The phonon spectra

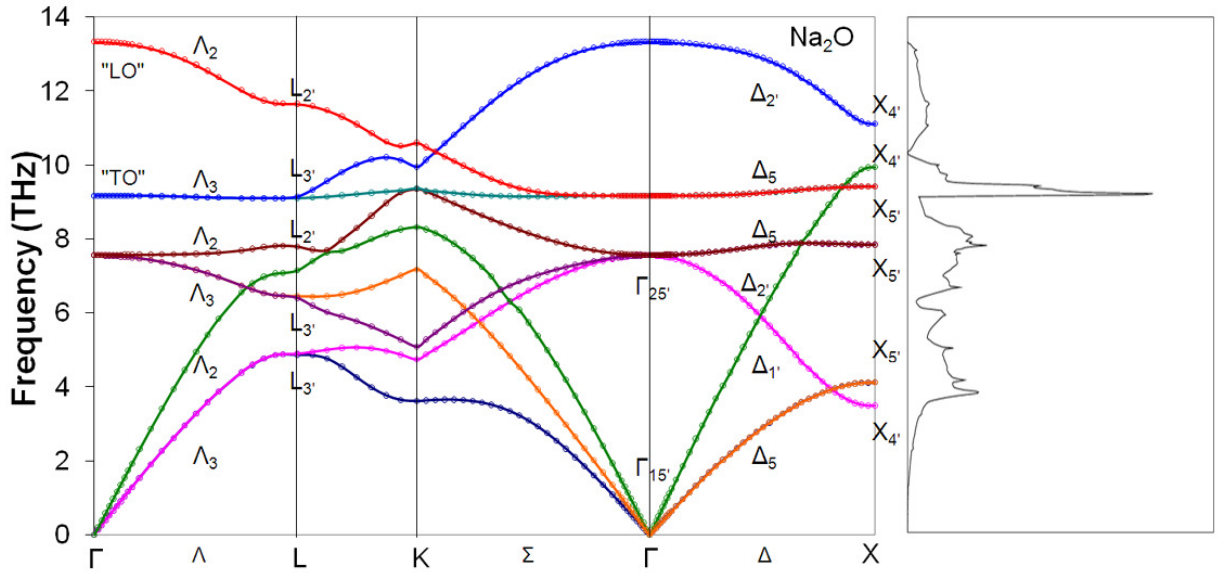

Figure 3.2: Phonon spectra along lines of high symmetry and pDOS from the LDA calculations. Color shown follows the continuous crossing of the modes of different symmetries. Notation along colored lines denotes symmetries as originally proposed by Bouckaert, Smoluchowski and Wigner [25].

displays nine modes, as expected for a material with three atoms in a unit cell. The three lowest frequency modes are the acoustic modes while the remaining six higher frequency modes are the

optical modes. Our results are consistent with central-zone frequencies for the two lowest transverse optical modes calculated by Dovesi; however, no other calculated or experimental data exists for comparison.

3.3.1 Acoustic Wave Velocities, Elastic Constants and Bulk Moduli

Analysis of the acoustic modes in the linear regime near the Γ point allows calculation of both longitudinal and transverse acoustic velocities:

$$\boldsymbol{v} = \frac{d\boldsymbol{\omega}}{d\boldsymbol{k}}$$

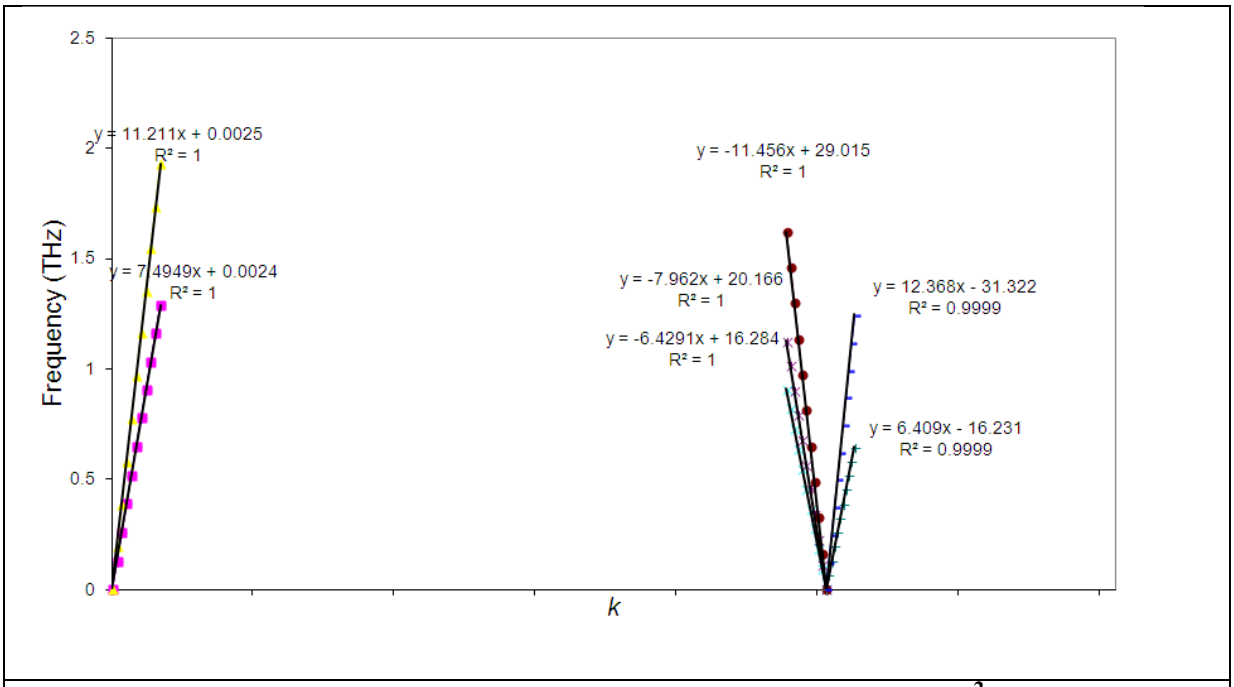

Figure 3.3.1: Acoustic modes in linear regime with fit equations and R^2 values displayed

Figure 3.3.1 shows the acoustic modes near the Γ point fit with linear equations and R^2 values. To get to velocity from the fits, the slope of the line (in Hz) is simply multiplied by the lattice parameter (in m). Our calculated acoustic velocities are presented in Table 3.3.

Recall that in a cubic crystal, the only non-zero elastic moduli are C_{11}, C_{12}, and C_{44}. Customarily, when using DFT to calculate elastic constants, the equilibrium structure is distorted by applying small normal and shear strains then calculating the stress tensor. Varying the magnitude of the strains allows derivation of elastic constants from the stress-strain relationship. However, these calculations can become cumbersome and computationally expensive very quickly. In our calculations, we use the known relationships between elastic constants and acoustic velocities [26] to derive the elastic constants and bulk modulus from the acoustic velocities calculated from the phonon spectra.

In the [100] direction, the transverses acoustic modes are degenerate and two equations relate elastic constants with acoustic velocity:

$\omega^2\rho = C_{11}k^2$(longitudinal)

$\omega^2\rho = C_{44}k^2$ (transverse);

in the [110] direction, the transverse waves are not degenerate, so three equations relate elastic constants with the acoustic velocity:

$\omega^2\rho = \frac{1}{2}(C_{11} + C_{12} + 2C_{44})k^2$ (longitudinal)

$\omega^2\rho = C_{44}k^2$ (transverse)

$\omega^2\rho = \frac{1}{2}(C_{11} - C_{12})k^2$ (transverse);

and, in the [111] direction, the transverse waves are also degenerate, so we again have two equations:

$$\omega^2\rho = \frac{1}{3}(C_{11} + 2C_{12} + 4C_{44})k^2 \text{(longitudinal)}$$

$$\omega^2\rho = \frac{1}{3}(C_{11} - C_{12} + C_{44})k^2 \text{ (transverse).}$$

Where, ρ is the density per unit cell, ω is the frequency and k is the wave vector. These seven relationships give us an overdetermined system of equations. In order to find the elastic constants, we calculated $v^2\rho$ for all of the acoustic modes and found least squares solutions for C_{11}, C_{12}, and C_{44} using Excel Solver. Table 3.3.details the acoustic velocities and elastic constants with associated errors.

		LDA	**GGA**	**Table 3.3: Acoustic velocities and elastic constants from phonon spectra. Numbers in parenthesis are errors associated with fitting.**
Velocities ($10^3\frac{m}{s}$)	v_{100LA}	6.679	6.442	
	v_{100TA}	3.461	3.080	
	v_{110LA}	5.832	5.707	
	v_{110TA1}	3.723	3.022	
	v_{110TA2}	4.054	4.045	
	v_{111LA}	6.990	6.619	
	v_{111TA}	4.673	4.584	
C_{ij} (GPa)	C_{11}	114(8)	114(7)	
	C_{12}	37.8(1.3)	34.7(1.3)	
	C_{44}	32.8(0.6)	27.4(0.5)	

While there are no experimental data with which to compare our results, our calculations are in reasonable agreement with those of Dovesi *et al*[6]: 126.3 GPa (C_{11}), 23.0 GPa (C_{12}) and 37.8 GPa (C_{44}). Another good test of the validity of our elastic constants and acoustic velocities from phonon spectra is to calculate the bulk modulus from elastic constants:

$$K = \frac{1}{3}(C_{11} + 2C_{12})$$

and compare the results with other calculations. Table 3.4 provides a comparison of our K calculated from both elastic constants and from the second derivative of total energy with respect to volume with those calculated in other studies. Our K values calculated from the volume are low compared to other calculations, but those calculated with acoustic velocities are within fitting error of those calculated by others [6, 7, 9].

	Method		**K (GPa)**
This Study	LDA	From C_{ij}	63(4)
		From $\frac{d^2E}{dV^2}$	56
	GGA	From C_{ij}	61(3)
		From $\frac{d^2E}{dV^2}$	54
Eithiraj [9]	TB-LMTO		59
Dovesi [6]	LCAO		58
Shukla [7]	HF		61.1

Table 3.4:

Comparison of calculated bulk moduli (K) from this study and others.

3.3.2 Thermodynamic Parameters

Using elastic constants and the pDOS from phonon calculations, we can calculate some thermodynamic parameters for Na_2O under the harmonic approximation. In the harmonic approximation, the specific heat is defined as:

$$C(T) = \frac{\hbar_B}{V_{cell}} \int_0^\infty d\Omega \mathcal{D}(\Omega) \left(\frac{\hbar\Omega / 2\hbar_B T}{sinh\left(\hbar\omega / 2\hbar_B T\right)} \right)^2$$

Where (Ω) is the density of states and V_{cell} is the cell volume. The pDOS is normalized as $3n = \int d\Omega \mathcal{D}(\Omega)$, where n is the number of atoms per unit cell, 3 for Na_2O. At low temperature, the pDOS scales as Ω^2, with a coefficient that depends on the elastic constants. The corresponding specific heat is:

$$C(T) = \left(\frac{12\pi^4 n \hbar_B}{5V_{cell}} \right) \left(\frac{T}{\Theta_D} \right)^3$$

The Debye temperature (Θ_D) is related to the elastic constants through a complicated angular average. An approximate version of this angular average is known to work well with cubic insulators at low temperature [27]:

$$\Theta_0 = C_{av} \left(\frac{aG_{av}}{M} \right)^{1/n};$$

$$G_{av} = \left\{ C_{44} \left[\frac{(C_{11} - C_{12})C_{44}}{2} \right]^{1/2} \left(\frac{C_{11} - C_{12} + C_{44}}{3} \right) \right\}^{1/3} 3$$

Here, Θ_0 is the low temperature Debye temperature, M is the average atomic weight and *a* is the lattice parameter. Both C_{av} and *n* are empirically derived model parameters which, for f.c.c.

insulators are set to 18.56 K and 2, respectively. We find Θ_0 = 559K for LDA and 545K for GGA. From this we can predict specific heat for temperatures less than Θ_0. At higher temperatures, the factor $\frac{\hbar\Omega}{2k_B T}$ is small over the whole spectrum and the specific heat is the DuLong-Petit value:

$$C(T) = \frac{3nk_B T}{V_{cell}}.$$

It is also useful to define the moments, $\langle\omega^n\rangle$ of the pDOS spectrum and characteristic temperatures T_n. These can be calculated by:

$$\langle\omega^n\rangle = \left(\frac{k_B T_n}{\hbar}\right)^n = \frac{\int d\Omega \mathcal{D}(\Omega)\Omega^n}{\int d\Omega \mathcal{D}(\Omega)}$$

Then, the harmonic specific heat can be Taylor expanded at high T, giving the first correction:

$$C(T) = \frac{3nk_B}{V_{cell}}\left[1 - \frac{1}{12}\left(\frac{T_2}{T}\right)^2 + \cdots\right]$$

From our predicted spectrum, we find T_2 = 377 K for LDA.

Another important quantity is the absolute harmonic entropy, which can be written as

$$S = 3Nk_B log\left(\frac{T}{T_{log}}\right)$$

The logarithmic temperature is defined: $k_B T_{log} = \hbar\omega_{log}$, where the logarithmic average is the limit as $n \to 0$ of $\langle\omega^n\rangle^{\frac{1}{n}}$, or

$$\omega_{log} = \exp\langle\log\omega\rangle$$

For the LDA, we find T_{log} = 332 K.

Chapter 4. Conclusion

Sodium and its oxide, Na_2O play an important role in the Earth Sciences. They are found in abundance in both crustal and mantle minerals. Additionally, Na_2O, with its cubic antifluorite crystal structure, is a candidate material for solid state batteries, fuel cells and gas detectors. Up until recently, very little data existed for this important material. Recent computational experiments have done little to add to the existing data, focusing instead on validating new computational methodology. In the current study, we have used the well tested Density Functional Theory to present new data on Na_2O . We calculated the lattice parameter, cohesive energy, bulk modulus and electronic band structure for comparison with other data and reported new data including phonon spectra and phonon density of states, elastic constants and thermodynamic parameters such as harmonic entropy and the low temperature Debye temperature (Θ_0) [10]. Our calculations are in good agreement with experimental and computational data, where data exist. All electronic structure calculations were performed by Meagan Thompson with guidance from Xiao Shen. Thermoelastic parameters, excluding Θ_0, were calculated by Phil Allen; Θ_0 calculated by Meagan Thompson.

References:

1. Lide, D., *CRC Handbook of Chemistry and Physics, 88th Edition (Crc Handbook of Chemistry and Physics)*. 2007: CRC.
2. Faure, G., *Principles and applications of geochemistry: a comprehensive textbook for geology students*. 1998, Upper Saddle River, N.J.: Prentice hall.
3. Zintl, E., A. Harder, and B. Dauth, *Gitterstruktur der Oxyde, Sulfide, Selenide und Telluride des Lithiums, Natriums und Kaliums.* Zeitschrift für Elektrochemie und angewandte physikalische Chemie, 1934. **40**(8): p. 588-593.
4. Weast, R.C., *CRC Handbook of Chemistry and Physics, 67th Edition* 1986-1987: CRC, Cleveland, OH.
5. Barrie, A. and F.J. Street, *An Auger and X-ray photoelectron spectroscopic study of sodium metal and sodium oxide.* Journal of Electron Spectroscopy and Related Phenomena, 1975. **7**(1): p. 1-31.
6. Dovesi, R., et al., *On the elastic properties of lithium, sodium and potassium oxide. An ab initio study.* Chemical Physics, 1991. **156**(1): p. 11-19.
7. Shukla, A. and M. Dolg, *Towards a quantum-chemical description of crystalline insulators: A Wannier-function-based Hartree-Fock study of Li_2O and Na_2O.* Journal of Chemical Physics, 1998. **108**(20): p. 8521.
8. Mikajlo, E.A. and et al., *Electron momentum spectroscopy and linear combination of atomic orbitals calculation of bulkÂ Na 2 O.* Journal of Physics: Condensed Matter, 2003. **15**(13): p. 2155.
9. Eithiraj, R.D., G. Jaiganesh, and G. Kalpana, *Electronic structure and ground-state properties of alkali-metal oxides-Li2O, Na2O, K2O and Rb2O: A first-principles study.* Physica B: Condensed Matter, 2007. **396**(1-2): p. 124-131.
10. Thompson, M., X. Shen, and P.B. Allen, *Density functional calculation of electronic structure and phonon spectra of Na_{2}O.* Physical Review B, 2009. **79**(11): p. 113108.
11. Kohanoff, J. and N.I. Gidopoulos, *Density Functional Theory: Basics, New Trends and Applications*, in *The Handbook of Molecular Physics and Quantum Chemistry*, E.S. Wilson, Editor. 2002, John Wiley and Sons.
12. Kohn, W., A.D. Becke, and R.G. Parr, *Density Functional Theory of Electronic Structure.* The Journal of Physical Chemistry, 1996. **100**(31): p. 12974-12980.
13. Ohno, K., K. Esfarjani, and Y. Kawazoe, *Computational Materials Science: From Ab Initio to Monte Carlo Methods*. Solid-State Sciences ed. Springer. Vol. 129. 1999.
14. Magyari-Kope, B., *Structural Stability of Solids from First Principles Theory, Ph. D. Dissertation*, in *Department of Physics*. 2002, Royal Institute of Technology: Stockholm. p. 61.
15. Sutton, A.P., *Electronic structure of materials*. 1993: Clarendon Press.
16. Wentzcovitch, R.M. and L. Stixrude, *Theoretical and computational methods in mineral physics : geophysical applications*, Chantilly, Va.: Mineralogical Society of America.
17. Hohenberg, P. and W. Kohn, *Inhomogeneous Electron Gas.* Physical Review, 1964. **136**(3B): p. B864-B871.
18. Levy, M., *Universal variational functionals of electron densities, first-order density matrices, and natural spin-orbitals and solution of the v-representability problem.* Proceedings of the National Academy of Sciences, 1979. **76**(12): p. 6062-6065.

19. Jones, R.O. and O. Gunnarsson, *The density functional formalism, its applications and prospects.* Reviews of Modern Physics, 1989. **61**(3): p. 689-746.
20. Perdew, J.P., K. Burke, and M. Ernzerhof, *Generalized Gradient Approximation Made Simple*. Physical Review Letters, 1996. **77**(18): p. 3865-3868.
21. Giannozzi, P., et al. *http://www.quantum-espresso.org*.
22. Vanderbilt, D., *Soft self-consistent pseudopotentials in a generalized eigenvalue formalism.* Physical Review B, 1990. **41**(11): p. 7892-7895.
23. Perdew, J.P. and A. Zunger, *Self-interaction correction to density-functional approximations for many-electron systems.* Physical Review B, 1981. **23**(10): p. 5048-5079.
24. http://en.wikipedia.org/wiki/File:Brillouin_Zone_%281st, F.s. [cited 2011 December 1]; Brillouin zone for face centered cubic lattice. Licensed as an uncopywritten public domain image.].
25. Bouckaert, L.P., R. Smoluchowski, and E. Wigner, *Theory of Brillouin Zones and Symmetry Properties of Wave Functions in Crystals.* Physical Review, 1936. **50**(1): p. 58-67.
26. Landau, L.D., et al., *Theory of elasticity*. 1986: Butterworth-Heinemann.
27. Siethoff, H. and K. Ahlborn, *The Dependence of the Debye Temperature on the Elastic Constants.* physica status solidi (b), 1995. **190**(1): p. 179-191.